

JEAS



JOURNAL OF ENGINEERING — AND — APPLIED SCIENCES

A Refereed Academic Journal Published by the
Publishing and Translation Center at Majmaah University

Vol. 5 Issue (1)

(May 2018)

ISSN: 1658 - 6638



**IN THE NAME OF ALLAH,
THE MOST GRACIOUS,
THE MOST MERCIFUL**

**Kingdom of Saudi Arabia
Ministry of Education
Majmaah University**



JEAS

JOURNAL OF
ENGINEERING
— AND —
APPLIED SCIENCES

**A Refereed Academic Journal Published by the
Publishing and Translation Center at Majmaah University**

Vol. 5, Issue (1)

(May 2018)

ISSN: 1658 - 6638



Publishing & Translation Center - MU

About the Journal

Journal of Engineering and Applied Sciences (JEAS)

Vision

Pioneer journal in the publication of advanced research in engineering and applied sciences.

Mission

A peer-review process which is transparent and rigorous

Objectives

- a) Support research that addresses current problems facing humanity.
- b) Provide an avenue for exchange of research interests and facilitate the communication among researchers.

Scope

JEAS accepts articles in the field of engineering and applied sciences. Engineering areas covered by JEAS include:

Engineering areas

Architectural Engineering
Chemical Engineering
Civil Engineering
Computer Engineering
Electrical Engineering
Environmental Engineering
Industrial Engineering
Mechanical Engineering

Applied Sciences areas

Applied Mathematics
Applied Physics
Biological Science
Biomathematics
Biotechnology
Computer Sciences
Earth Science
Environmental Science

Correspondence and Subscription

Majmaah University, Post Box 66, Al-Majmaah 11952, KSA

email: jeas@mu.edu.sa

© Copyrights 2018 (1439 H) Majmaah University

All rights reserved. No part of this Journal may be reproduced or any electronic or mechanical means including photocopying or recording or uploading to any retrieval system without prior written permission from the Editor-in-Chief.

All ideas herein this Journal are of authors and do not necessarily express about the Journal view

Journal of Engineering and Applied Sciences

Editorial Board

Dr. Tawfeeq Abdullah Alkanhal
Editor-in-Chief

Associate Professor of Computer Engineering, College of Engineering,
Majmaah University

Dr. Thamer Shuleih Alharbi
Member

Associate Professor of Physics, College of Science,
Majmaah University

Dr. Sameh Saadeldin Ahmed
Manager

Associate Professor of Civil and Environmental Engineering,
College of Engineering, Majmaah University

Editorial

Scientific publishing has brought many challenges to authors. With increasing number of scientific journals, varying scopes and reviewing requirements, and cost of publishing to authors, finding the right journal to publish an article is a decision many authors must bitterly confront and resolve. The publication of scientific findings is an integral part of the life of researchers; and the process of publishing has evolved to become an efficient system of decimating knowledge and collaboration among scientists. Science journals have institutionalized procedures to manage large volume of article submissions per year; in many cases, journals began to define narrower scopes for a dual purpose: managing submissions and delivering outstanding research.

Based on recent studies, the scientific publishing world consists of more than 25 thousands active journals in various disciplines and fields. Science Direct hosts 3,348 journals (as of February 2014). The Directory of Open Access Journals lists in its search engine more than 9,800 open access online journals.

According to recent estimates, the number of scientific journals grows by 3% per year worldwide. With this large number of journals, journals may find it harder to stay afloat.

In its inauguration, the board of editors is honored to introduce to the scientific community the Journal of Engineering and Applied Sciences - JEAS, another scientific journal from Majmaah University. The board has pledged a commitment to JEAS authors and readers to bring the most dynamic and vibrant journal management with better satisfaction.

Dr. Tawfeeq Alkanhal

Contents

Editorial.....	vii
-----------------------	------------

ORIGINAL ARTICLES

Improved Performance of Doppler Tolerant Radars Using Digital Code <i>Saud S. Alotaibi</i>	1
Simulation Study on Charged Particle Discrimination Properties of CdTe Detectors <i>T. Alharbi</i>	7
Parametric Analysis of Diesel-Brayton Combined Cycle <i>M.N.Khan</i>	12

Improved Performance of Doppler Tolerant Radars Using Digital Code

Saud S. Alotaibi

Department of Information Systems, College of Computer and Information Systems,

Umm - AlQura University, Makkah, Saudi Arabia.

ssotaibi@uqu.edu.sa

ABSTRACT:

Radio Detection and Ranging (RADAR) finds huge application in navigation to detect the speed velocity, angle, and range of the objects such as ships, aircraft, automobiles, missiles and it is also used for determining the environmental and geographical conditions. This vast application of Radar Engineering diverts the attention of the research community to work on this era. It has some issues and challenges such as low probability of target detection, the effect of noise is high, time complexity is more with poor resolution. Hence, for accurate detection ambiguity should be improved. In the current literature, various authors presented the models to increase the autocorrelation by using either compression techniques or by improving the merit factor. However, these approaches concentrate on static objects, have noise peaks which are above the threshold limit at various Doppler frequencies and can hide the targets easily. In this paper, Linear Block Code (LBC) has been used which improves the performance of radar and create clear windows at desired Doppler to give the accurate information about the moving target with respect to its speed and position. The 256-bit matrices code is designed and tested using MATLAB.

Keywords: Radar, linear code, Doppler Effect, target detection, MATLAB

Introduction

Radar is used for object detection by broadcasting electromagnetic waves towards the object and receiving the echoes from it. The strength of the received signal determines characteristics such as angle, distance, and speed of the desired object in the multi-target environment. Radar finds huge application in battlefields, detecting geographical structures, aircraft, ships, and automobiles. Radar consists of a duplex channel, a transmitter, and a receiver. In general, the transmitter acts as a receiver during certain allocated time intervals for pulse wave radar. But there are some limitations associated with it such as poor resolution, short range, and the effect of noise and lack of accuracy in target detection.

The state-of-art developed various pulse compression techniques and methods to improve the merit factor to obtain high-resolution radar and increase the probability of object detection in a multi-target environment. If the radar is capable of precisely sensing the target and determining its range and speed in the multi-object environment, then it is said to be high-resolution radar. The pulse compression techniques employ digital codes such as Barker codes, Goley and polyphase codes to obtain high-resolution radar and are restricted to static object detection. Coding techniques are used to detect the target position by auto-correlating the received signals with the transmitted signals. The range and velocity of the object

can be determined in terms of delay and Doppler shift. Improving the merit factor comparatively increases the noise which hinders the probability of object detection. In multi-target environments, the echoes are overlapped from the targets probing difficulties to detect them and individual objects are not viewed clearly as each object possesses its own path and velocity. Hence, it becomes important to judge the object in such environments

Range resolution is a critical parameter related to radar. The range can be measured using the formula $R_o = c \times T_p / 2$, where 'c' is the velocity of light, 'T_p' is the pulse width and division with 2 is done to take single direction, as it is to and fro process. This formula is valid for simple pulse radar but for high range resolution radar, short pulses are used. This radar requires high energy pulse and peak powers.

In this paper, Linear block codes are considered to generate digital codes of 256-bit matrices and are transmitted to obtain clear windows at desired Doppler frequencies and increase the probability of detecting the object in multi-object environments with noise amplitude less than the threshold limit (0.2, normalized amplitude). LBC are used for encoding the data and are readily available in any digital communication system there is no need for additional infrastructure for the code designed in the presented approach. However, one can use any of the available digital codes such as (6, 3), (7, 4), and so on. In the proposed approach (7, 4) code which is used for generating 256 bits matrices.

The rest of the paper is organized as follows, in section 2 related work is presented, the proposed approach and comparative analysis are discussed in section 3, and the paper is concluded in section 4.

Related Work

There are numerous works done in the field of radar to improve the range resolution and reduce the undesirable noise. Deng, 1996 developed the sequences with good auto-correlation and cross-correlation properties. These sequences are optimized using an optimization algorithm to improve the resolution and reduce the noise. However, high resolutions may not be possible as sequence lengths are limited. The author in Deng, (2004) discussed the design of poly-phase codes by employing a hybrid optimization algorithm for orthogonal netted radar. But the design of poly-phase codes increases the complexity and there is no significant reduction in noise which may degrade the performance of radar. The authors Bo Liu (2006) and Sharma (2012) presented an approach in which they developed poly-phase codes for MIMO radar systems based on the algebraic method. The method may increase the complexity of the system.

Sufiyan and Vinay (2013) developed Doppler tolerant poly-phase codes based on step approximation technique using hyperbolic frequency modulation and p1, p3 frank code. The codes give better results than barker and frank codes but have a limited length which may restrict the high-resolution factor of the radar. Kretschmer and Welch (2000) employed weighting schemes to p4 poly-phase codes for pulse compression technique in radars to reduce the sidelobe noise. However, there is a loss of resolution which makes this method unsuitable for designing high-resolution radar. Luszczuk, and Mucha (2008) presented a weighting technique called Kaiser-Bessel window function of amplitude to reduce the side noise. Though this method is better than the Hamming window function, it may fail to decrease the noise below threshold noise level with high resolution. Reddy and Anuradha(2015) discussed two optimal windowing functions namely Kaiser-Hamming and Cosh-Hamming techniques to improve the signal to noise ratio (SNR) and improve the performance of Mesosphere-Stratosphere-Troposphere (MST) radar systems.

Tian et al.(2017) presented an approach to improve the range resolution in radars using stepped frequency and phase-coded signals with orthogonal frequency division multiplexing technique (OFDM). But there may be complex as OFDM is sensitive to Doppler shift and high peak to average power ratio. Neon and Joel (2017) discussed a pulse compression technique for Doppler tolerant radar using modified p4.

They combined linear frequency modulation with a p4 coding method to reduce the side noise and improve resolution in radar. However, the side lobes are more than the threshold limit which can mask small moving targets. Singh et al (2016) presented a re-sampling windowing technique using binary hex code to improve the resolution and reduce the noise in Doppler tolerant radar. But the noise still persists above the threshold level. Aleem et al.(2019) designed a code based on ASCII codes to reduce the noise in and obtain high resolution in the multi-target environment at desired Doppler frequencies. In the presented approach LBC (7, 4) is used to generate 256 bits code matrix which reduces the side noise below the threshold level and improves the range resolution.

Proposed Technique

Linear codes are generally used for error correction at the receiver end in communication systems. In the presented approach (7, 4) code is considered. However, one can select any of the available digital codes according to their desired code length. In this paper, a 256 bits code is designed for object detection and obtaining high resolution at desired Doppler frequencies. The proposed approach can be implemented using the following steps:

1. Generation of 16 radar codes of 7-bit length using (7, 4) linear block code.
2. Add even or odd parity bit to the radar codes obtained in step 1 to make the code length equal to 8-bits. Hence 16 codes of 8-bit length are developed.
3. The matrix form of step 2 is of order 16(codes) \times 8(bits), to make this matrix equal in order (i.e. 16 \times 16 square matrix of 256 bits) the complement form of 8 bits obtained at step 2 is concatenated to the 8-bits of step 2.
- 4.

The digital code (7, 4) contains 4 radar bits and the radar code of 7 bits is generated using radar bits matrices B_{-R_i} (where $i = 0, 1, 2, 3, \dots, 15$) which is four-bit binary representation of 0-15 decimal numbers (i.e. $B_{-R_0} = [0000]$, $B_{-R_1} = [0001]$, $B_{-R_2} = [0010]$, ..., $B_{-R_{15}} = [1111]$) and multiplying each of them with radar generator matrix G_{-R} represented as;

$$G_R = \begin{pmatrix} 1 & 0 & 0 & 0 & 1 & 1 & 1 & 1 \\ 0 & 1 & 0 & 0 & 1 & 1 & 1 & 0 \\ 0 & 0 & 1 & 0 & 1 & 0 & 1 & 0 \\ 0 & 0 & 0 & 1 & 0 & 1 & 1 & 1 \end{pmatrix} \dots\dots(1)$$

Note that the generator matrices are available with each of the linear block codes. The B_{-Ri} is multiplied (using modulo-2 addition) with G_{-R} to generate radar codes C_{-Ri} is represented as

$$C_{Ri} = B_{Ri} \times G_R$$

For example, when $i=0$

$$C_{R0} = B_{R0} \times G_R$$

$$= [0000] \times \begin{bmatrix} 1000111 \\ 0100110 \\ 0010101 \\ 0001011 \end{bmatrix} \dots(2)$$

$$C_{R0} = [00000000]$$

Similarly, all the remaining radar codes are generated using (1). Therefore, 16 radar codes of length 7 bits are generated and 8th bit of the code is obtained either by even parity or odd parity of the radar code as in Table 1 and Table 2 respectively to produce initial radar bits (of 8-bit length). Hence, there are 32 initial radar codes (I_{-Rj}) i.e. I_{-R0} - I_{-R31} (16 with even parity + 16 with odd parity) of 8 bit length, where $j=0, 1, 2, \dots, 31$.

These initial radar codes are divides into two folds

1. Even parity fold
2. Odd parity fold

Radar codes (C_{R0} - C_{R15})	Even Parity	I_{Rj} (j= 0 -15)
0000000	0	00000000
0001011	1	00010111
0010101	1	00101011
0011110	0	00111100
0100110	1	01001101
0101101	0	01011010
0110011	0	01100110
0111000	1	01110001
1000111	0	10001110
1001100	1	10011001
1010010	1	10100101
1011001	0	10110010
1100001	1	11000011
1101010	0	11010100
1110100	0	11101000
1111111	1	11111111

Radar codes (C_{R0} - C_{R15})	Odd parity	I_{Rj} (j=16 -31)
0000000	1	00000001
0001011	0	00010110
0010101	0	00101010
0011110	1	00111101
0100110	0	01001100
0101101	1	01011011
0110011	1	01100111
0111000	0	01110000
1000111	1	10001111
1001100	0	10011000
1010010	0	10100100
1011001	1	10110011
1100001	0	11000010
1101010	1	11010101
1110100	1	11101001
1111111	0	11111110

EVEN PARITY FOLD

In this fold, we consider the first 16, 8-bit initial radar codes (I_{-R0} - I_{-R15}) refer to Table 1. Hence the 16×8 matrix of 128-bits is generated. To make this matrix equal (square matrix) to 256-bits we take the complement of each radar code and concatenate it to un-complemented radar code represented as

$$F_{Rj} = I_{Rj} \overline{I_{Rj}} \quad (3)$$

where F_{-Ri} is the final j^{th} 16- bit radar code I_{-Rj} is the j^{th} radar code (8-bit) ($\overline{I_{-Rj}}$) is the complement of I_{-Rj} (8-bit) and in this fold $j= 0, 1, 2, \dots, 15$. The 16×16 matrix is generated by taking F_{-Rj} as rows of the matrix (refer to Table 3)

Table 3 matrix is tested using MATLAB for ambiguity function. Figure 1 shows the Ambiguity function (variation in Doppler with amplitude of the received signal) of even parity fold. From the figure, it is observed that there are clear windows from 3-9 kHz and 11-40 kHz where the side lobe noise is approximately 0.1 and the overall sidelobe noise is less than the threshold value (i.e. 0.2). Therefore, a target cannot be masked in the side noise of a single object and can detect it accurately in multi-object environments. Figure 2 shows a variation of the delayed signal along with the Doppler. As the 256-bit code is transmitted a high resolution is obtained at the receiver end.

TABLE 3. EVEN PARITY FOLD MATRIX OF 256 BITS (j= 0, 1, 2,..., 15)

	I_{Rj}								$\overline{I_{Rj}}$							
F_{R0}	0	0	0	0	0	0	0	0	1	1	1	1	1	1	1	1
F_{R1}	0	0	0	1	0	1	1	1	1	1	1	0	1	0	0	0
F_{R2}	0	0	1	0	1	0	1	1	1	1	0	1	0	1	0	0
F_{R3}	0	0	1	1	1	1	0	0	1	1	0	0	0	0	1	1
F_{R4}	0	1	0	0	1	1	0	1	1	0	1	1	0	0	1	0
F_{R5}	0	1	0	1	1	0	1	0	1	0	1	0	0	1	0	1
F_{R6}	0	1	1	0	0	1	1	0	1	0	0	0	1	1	0	0
F_{R7}	0	1	1	1	0	0	0	1	1	0	0	0	1	1	1	0
F_{R8}	1	0	0	0	1	1	1	0	0	1	1	1	0	0	0	1
F_{R9}	1	0	0	1	1	0	0	1	0	1	1	0	0	1	1	0
F_{R10}	1	0	1	0	0	1	0	1	0	1	0	1	1	0	1	0
F_{R11}	1	0	1	1	0	0	1	0	0	1	0	0	1	1	0	1
F_{R12}	1	1	0	0	0	0	1	1	0	0	1	1	1	1	0	0
F_{R13}	1	1	0	1	0	1	0	0	0	0	1	0	1	0	1	1
F_{R14}	1	1	1	0	1	0	0	0	0	0	0	1	0	1	1	1
F_{R15}	1	1	1	1	1	1	1	1	0	0	0	0	0	0	0	0

Odd Parity Fold

In this fold the initial radar codes obtained in Table 2 is considered (i.e. from I_{R16} - I_{R31}) which will become the matrix of order 16×8 . Similar to even parity fold, the 256-bit square matrix is generated by concatenating the complement of 8-bits to the uncomplemented 8-bits represented as in(3). The only difference is that in this fold j ranges from 16 -31 refer to Table 4.

Figure 3 represents the ambiguity graph of Doppler versus amplitude, with clear windows at Doppler frequencies 1-9 kHz and 11- 40 kHz with noise side lobes approximately equal to 0.1 and the overall noise is less than 0.2. Figure 4 represents the Doppler versus delay graph.

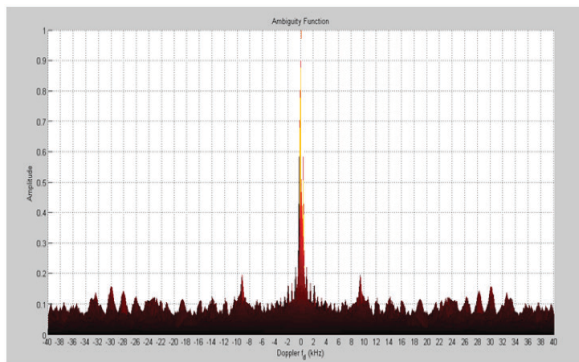


Fig. 1. Ambiguity function (Doppler versus Amplitude)

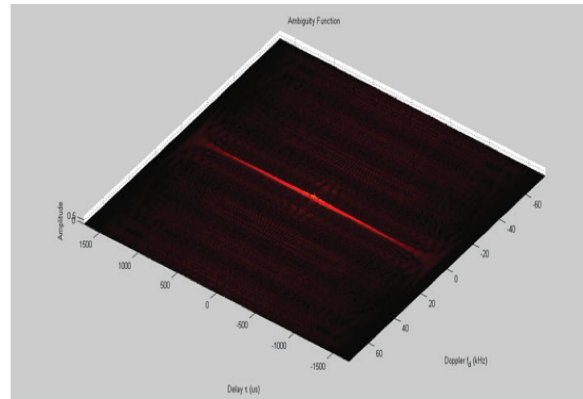


Fig. 2. Ambiguity function (Doppler versus Delay)

Comparative Analysis

The proposed approach is compared with the Barker codes, Golay codes, Singh codes, Singh et al, (2016) and Aleem codes Aleem *et al.*, (2019).

Shows the comparison of the proposed code with the existing codes used to reduce the side noise and improve the resolution. From the figure, it is observed that the presented approach has minimum noise peaks when compared to the traditional methods, this is because the proposed approach uses the orthogonality by using hamming bits in the desired code word. Barker and Golay's codes have a limited length which restricts the resolution of the radar with significant noise effect. Singh and Aleem codes have a good resolution as they make use of 256-bit code but still, noise amplitude is more when compared to the proposed approach as the proposed approach is simple and effectively reduce the noise. There is no ex-or gates employed when compared to Singh and Aleem's approaches.

TABLE 4. ODD PARITY FOLD MATRIX OF 256 BITS (j= 16, 17, ..., 31)

	I_{Rj}								$\overline{I_{Rj}}$							
F_{R16}	0	0	0	0	0	0	0	1	1	1	1	1	1	1	1	0
F_{R17}	0	0	0	1	0	1	1	0	1	1	1	0	1	0	0	1
F_{R18}	0	0	1	0	1	0	1	0	1	1	0	1	0	1	0	1
F_{R19}	0	0	1	1	1	1	0	1	1	1	0	0	0	0	1	0
F_{R20}	0	1	0	0	1	1	0	0	1	0	1	1	0	0	1	1
F_{R21}	0	1	0	1	1	0	1	1	1	0	1	0	0	1	0	0
F_{R22}	0	1	1	0	0	1	1	1	1	0	0	1	1	0	0	0
F_{R23}	0	1	1	1	0	0	0	0	1	0	0	0	1	1	1	1
F_{R24}	1	0	0	0	1	1	1	1	0	1	1	1	0	0	0	0
F_{R25}	1	0	0	1	1	0	0	0	0	1	1	0	0	1	1	1
F_{R26}	1	0	1	0	0	1	0	0	0	1	0	1	1	0	1	1
F_{R27}	1	0	1	1	0	0	1	1	0	1	0	0	1	1	0	0
F_{R28}	1	1	0	0	0	0	1	0	0	0	1	1	1	1	0	1
F_{R29}	1	1	0	1	0	1	0	1	0	0	1	0	1	0	1	0
F_{R30}	1	1	1	0	1	0	0	1	0	0	0	1	0	1	1	0
F_{R31}	1	1	1	1	1	1	1	0	0	0	0	0	0	0	0	1

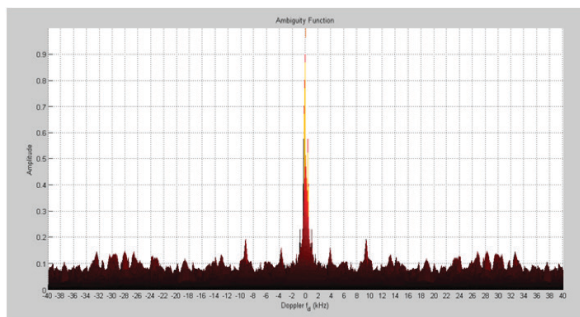


Fig. 3. Ambiguity function (Doppler versus Amplitude)

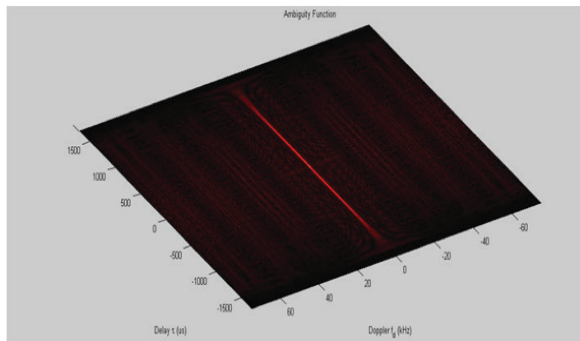


Fig. 4. Ambiguity function (Doppler versus Delay)

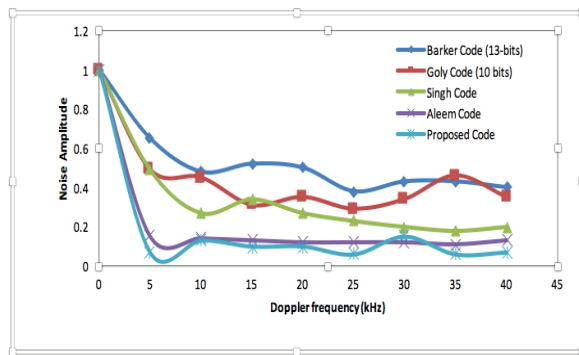


Fig. 5. Doppler versus Noise Amplitude

Conclusion

Radar Systems are very effective in object/target detection and tracking. The performance of these systems is degraded by noise and short-range resolution in multi-target environments. In the presented approach, a 256-bit code is designed which provides high range resolution and huge clear windows with noise below the threshold value and improve the probability of dynamic object detection in multi-target environments. The simulation results show that the designed codes provide clear windows over Doppler range of 0-40 kHz frequencies which is the practical band range employed in the existing radar communication systems. The proposed approach is simple and practically effective when compared to the conventional techniques.

Conflict of Interest

No conflict of interest.

References

- [1]. Deng, H. 1996. "Synthesis of binary sequences with good autocorrelation and crosscorrelation properties by simulated annealing", IEEE Transaction on Aerospace Electronic Systems, vol. 32, pp. 98-107
- [2]. H. Deng, 2004. "Polyphase code design for orthogonal netted radar systems", IEEE Transaction on Signal Processing, volume 52, issue 11, pp. 3126 3135
- [3]. Bo Liu, Zishu He, Jiankui Zeng, Benyong Liu, 2006. "Polyphase Orthogonal Code Design for MIMO Radar Systems", Proc. 2006 CIE International Conference on Radar
- [4]. Sharma G.V.K., Raja Rajeswari K, 2018 "Four Phase Orthogonal Code Design for MIMO Radar Systems",
- [5]. IEEE National Conference on Communications, NCC- 2012
- [6]. Syed Sufiyan Ahmed Rafiuddin, Vinay KumarBhangdia, 2013. "Empirical analysis on Doppler tolerant radar codes", International Journal of Scientific & Engineering Research, Volume 4, Issue 5, pp 1579-1582
- [7]. Kretschmer Jr. F. F. and Welch, L. R. 2000. "Side lobe Reduction Techniques for Polyphase Pulse Compression Codes", IEEE International Radar Conference, pp. 416-421
- [8]. Luszczek, M. and Mucha, D. 2008. «Kaiser-Bessel window weighting function for polyphase pulse compression code,» 17th International Conference on Microwaves, Radar and Wireless Communications, pp.1-4
- [9]. Ravi Krishna Reddy, D. and Anuradha, B. 2015 "Improved SNR Of MST Radar Signals By Kaiser-Hamming And Cosh-Hamming Window Functions," International Journal of Engineering Research and Applications, Vol. 5, Issue 3, pp.32-38 (Part -3)
- [10]. Xuanxuan Tian, Tingting Zhang, Qinyu Zhang, and Zhaohui Song, 2017. "HRR Profiling on Integrated Radar-Communication Systems Using OFDM-PCSF Signals". Hindawi Mathematical Problems in Engineering, Volume 2017, Article ID 5357187, 9 pages <https://doi.org/10.1155/2017/5357187>
- [11]. Neon S. de Jesus and Joel Joseph S. Marciano, 2017. "Doppler tolerant modified P4 code (DTMP4 code) for pulse compression radar". 2017 IEEE International Symposium on Signal Processing and Information Technology (ISSPIT) Doi: 10.1109/ISSPIT.2017.8388319
- [12]. Singh, R. K and Elizabeth Rani, D. and Syed Jalal Ahmad, 2016. "RSBHCWT: Re-Sampling Binary Hex Code Windowing
- [13]. Technique to Enhance Target Detection". Indian Journal of Science and Technology, vol 9(47), DOI: 10.17485/ijst/2016/v9i47/105952
- [14]. Aleem M., Singh R.P., Ahmad S.J. (2019), 2012 "Enhance Multiple Moving Target Detection in Doppler-Tolerant Radar Using IRAESC Technique". In: Saini H., Singh R., Patel V., Santhi K., Ranganayakulu S. (eds) Innovations in Electronics and Communication Engineering. Lecture Notes in Networks and Systems, vol 33. Springer, Singapore.

Simulation Study on Charged Particle Discrimination Properties of CdTe Detectors

T. Alharbi

Department of Physics, College of Science in Zulfi, Majmaah University, P.O. Box 1712, 11932, Saudi Arabia

t.alharbi@mu.edu.sa

ABSTRACT:

In this paper, a theoretical description of the shape of pulses initiated by α -particles and protons penetrating in planar cadmium telluride (CdTe) detectors is presented and the dependence of the shape of pulses on the energy of charged particles, as well as, the thickness of the detectors are discussed. The results of our calculations indicate that for protons and α -particles with energies above ~ 5 MeV a strong correlation exists between the specific ionization of the charged particles and the shape of output charge pulses, making planar CdTe detectors a promising candidate for the discrimination of charged particles in nuclear physics experiments.

Keywords: Charged particle detection; CdTe detectors; Pulse-shape discrimination

Introduction

Compound semiconductor detectors such as CdTe and CdZnTe detectors are widely used for x- and γ -ray measurement applications (Sordo *et al.*, 2009). The attraction of these materials is mainly due to their capability of operation at room temperature and their high quantum efficiency (Takahashi and Watanabe, 2001). Another interesting feature of these detectors is the strong dependence of the shape of output pulses upon the initial location of charge carriers in the detectors, resulting in a pulse-shape discrimination property. The dependence of the shape of pulses upon the initial location of charge carriers is resulted from a considerable difference in the drift mobilities of electrons and holes in compound semiconductors (Knoll, 2000 and Bargholtz *et al.* 1999) and it has been widely used for improving the spectroscopic and the timing performances of the detectors (see e.g. Ritcher and Siffert, 1992; Nakhoštin *et al.*, 2009), as well as, for position measurement applications (Nishizawa *et al.*, 2004). These detectors have been also considered for the detection of charged particles such as protons and α - particles in nuclear physics experiments (Rištinen *et al.*, 1981; Pearson *et al.*, 2000; Vincent *et al.*, 2002). The attraction of these detectors for charged particle detection is due to the possibility of building a compact charged particle detector array which can be fit inside an array of γ -ray detectors. In this way, a near 4π coverage around the target is possible, leading to an increased efficiency compared to identification methods which use mass separators to determine the mass over charge ratio of the recoiling nucleolus (Vincent *et al.*, 2002;

Dauids *et al.*, 1992). However, the dependence of the shape of output pulses on the specific energy-loss of charged particles is not very well known, while the pulse-shape discrimination property of these detectors may be very useful for selecting reaction channels by discriminating between charged particle reaction products. In this paper, the shapes of pulses from CdTe detectors induced by proton and α -particle have been calculated for different particle energies and detector thicknesses. The results of the pulse-shape calculations show a dependence of the pulse-shapes to the type of incident particles, indicating that CdTe detectors are a promising candidate for particle identification in nuclear physics experiments.

Pulse-shape calculation method

When a charged particle interacts with a semiconductor detector, equal number of electrons and holes are formed within a few picoseconds along the particle track. Under a uniform electric field in a planar detector, the electrons and holes move toward the electrodes, inducing a charge pulse on the electrodes which can be readout by using a charge-sensitive preamplifier. The shape of the leading edge of the induced charge pulse depends on the drift distances of the charge carriers from the electrodes of the detector, determined by the geometrical distribution of ionization in the detector (Bragg curve of the particle). To calculate the shape of charged particle induced pulses, we first consider the simple case in which the charge carriers are released in a point inside the detector. The shape of such pulse is calculated by using

the Hetch formula as (Hetch, 1932):

$$Q(t) = \frac{eNV}{d^2} \cdot \left\{ \mu_h \tau_h \left(1 - \exp\left(-\frac{t}{\tau_h}\right) \right) + \mu_e \tau_e \left(1 - \exp\left(-\frac{t}{\tau_e}\right) \right) \right\} \quad (1)$$

where N is the initial number of electron-hole pairs, V is the bias voltage, e is the electron charge, d is the detector thickness, μ is the charge carriers' mobility, τ is the charge carriers' lifetime, and e and h subscripts represent electrons and holes, respectively. The electrons and holes will only contribute to the function Q(t) during their drift times:

$$t_e = \frac{(d-x)d}{\mu_e V} \quad (2)$$

$$t_h = \frac{xd}{\mu_h V} \quad (3)$$

where x is the initial location of charge carriers. In our approach, for calculating the shape of charged particle induced pulses, i.e. when the charge carriers have a geometrical distribution in a CdTe detector, the detector's volume is divided into several thin slices and the pulse due to the drift of charge carriers from the center of each slice is calculated by using the Hetch formula. The total charge pulse is then obtained by adding up the charge pulses calculated for all the slices. This procedure is illustrated in Fig. 1. A planar CdTe detector is divided into 10 μm thick slices and the energy-loss of charged particles in each slice (ΔE) is calculated by using the TRIM Monte Carlo code (Ziegler and Biersck, 1985). The number of charge carriers in each slice is obtained as $\Delta E/w$, where w is the pair creation energy in CdTe. The pair creation energy in CdTe is 4.43 eV (Owen and Peacock, 2004). In the calculations, the lifetimes of electrons and holes were, respectively, set at $\tau_e=3 \times 10^{-6}$ second and $\tau_h=2 \times 10^{-6}$ second and the mobility of electrons and holes were, respectively, $\mu_e=1100 \text{ cm}^2/\text{Vs}$ and $\mu_h=100 \text{ cm}^2/\text{Vs}$ (Owen and Peacock, 2004).

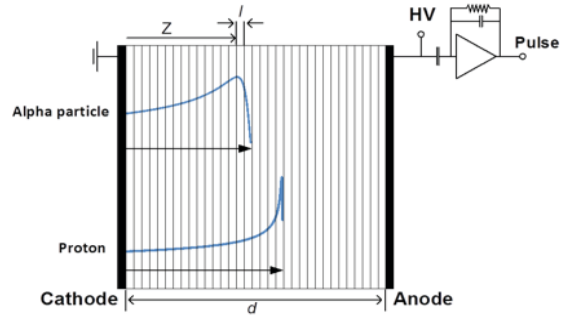


Fig. 1. Illustration of the calculation of a charge pulse from a planar CdTe detector for a charged particle. The CdTe detector is divided into 10 μm thin slices and the ionization in each slice is calculated by using the TRIM code. The Hetch formula is used to calculate the contribution of each slice to the charge pulse. The total charge pulse is then calculated by adding up the contributions from all the slices.

Results

Fig. 2 shows the calculated charge pulses for different slices of a 1 mm thick CdTe detector due to a 10 MeV proton. The proton hits the cathode side of the detector. It is seen that due to the smaller mobility of holes the contribution of holes to the pulses appears as a slope change in the leading edge of the pulses. This contribution increases with the depth of ionization in the detector. It is also apparent that three pulses, which are due to the ionization in the Bragg peak of the particle, have the largest contribution to the pulse. Another feature extractable from the shape of the pulses is that as the range of particles in the detector increases, the charge collection time increases which would have implications for count-rate limits and coincident relationships measurements. In the next step, the shapes of pulses for proton and α -particles stopping in a 1 mm thick CdTe detector were compared. The results of the comparison are shown in Fig. 3.

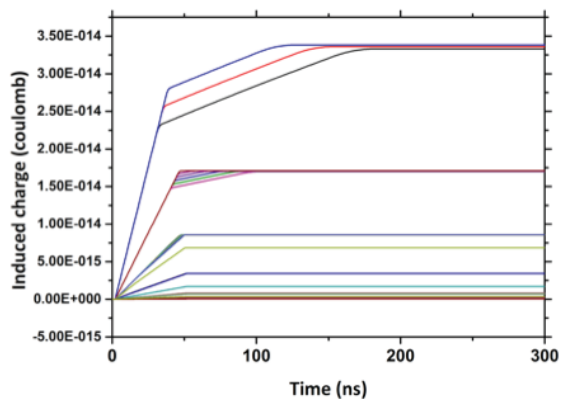


Fig. 2. Examples of charge pulses calculated for different slices of a 1 mm thick detector due to a 10 MeV proton. The proton penetrates the detector from the cathode side. The operating voltage is 100 volt.

In the calculations, the particles penetrate into the detector from the cathode side. The calculations were performed for particles with energies from 5 to 20 MeV. It is seen that for 5 MeV protons and α -particles the difference in the shape of charge pulses is negligible, but by increasing the energy of particles the difference in the shape of pulses increases so that for particles with energies above 10 MeV, the difference in the shape of the pulses is quite significant. The different shapes of the pulses for α -particles and protons of the same energy is due to the different contribution of electrons and holes in the output pulses, which is determined by the specific ionization of particles in the detector. The different geometrical distribution of charge carriers leads to different charge collection times in the detector which is reflected in the rise-time of the pulses. Calculations show that for 5 MeV protons and α -particles the difference in the locations of the Bragg peaks of the particles is only about 20 μm , and therefore, the difference in the shape of pulses is negligible. By increasing the energy of particles, the difference in the shape of pulses increases, though a larger level of charge trapping happens for the proton pulses due to the larger drift distance of holes in the detector.

The results of Fig. 3 indicate that the dependence of the shape of the pulses on the specific ionization of charged particles is significant for particles with energies above 10 MeV. However, the discrimination of particles with energies below 10 MeV is particularly desirable in nuclear physics experiments. Therefore, we calculated the shape of pulses for a different approach in which one particle (α -particle) stops in the detector while the other particle (proton) passes through the detector. This scenario is better illustrated in Fig. 4, where the calculated ranges of α -particles and protons in CdTe are shown. It is seen that the ranges of α -particles and protons in CdTe are quite different. This allows one to use thin detectors in which protons create the charge carriers along the crystal while charge carriers due to α -particles are limited close to the surface of the detector, leading to different charge collection times. As an example, the shapes of pulses for 5.5 MeV protons and α -particles in a 50 μm thick detector are shown in Fig. 5. The difference in the shape of the pulses can be characterized by a slope change in the last 20 ns of the proton pulse which is sufficiently long to be exploited for its identification. However, it should be mentioned that the minimum energy of charged particles that can be discriminated in this way is finally limited by the thickness of the detector because very thin detectors exhibit a large capacitance and are also difficult to be manufactured.

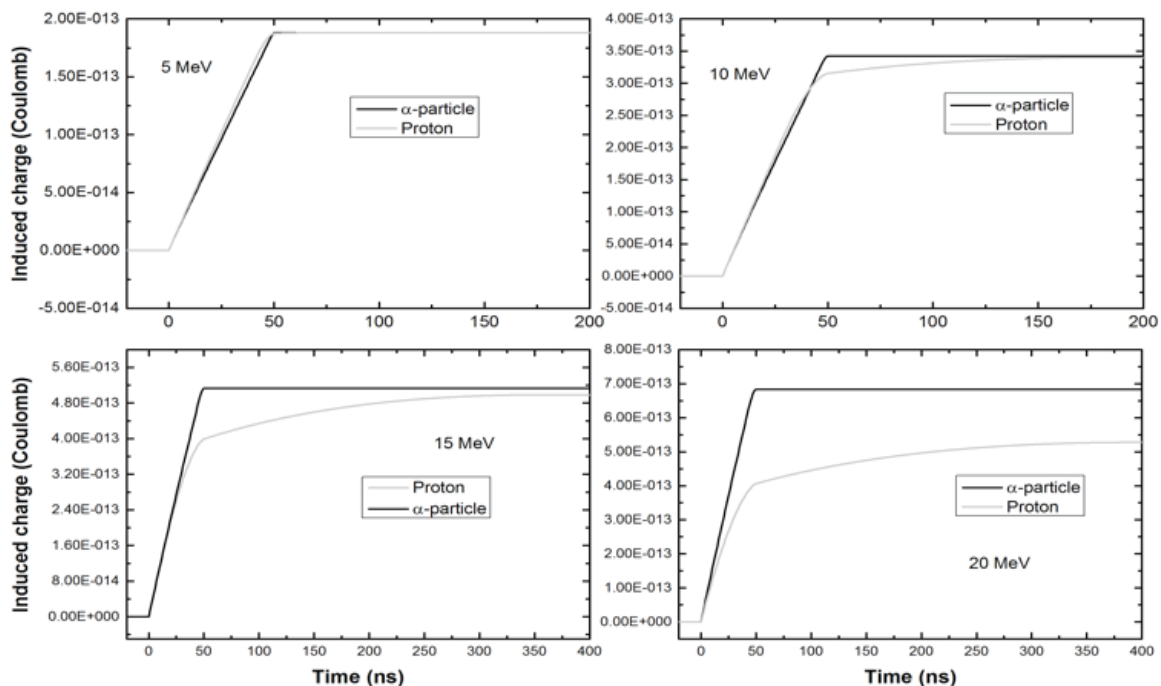


Fig. 3. The calculated pulses for proton and α -particles of 5, 10, 15 and 20 MeV impinging on a 1 mm thick CdTe detector.

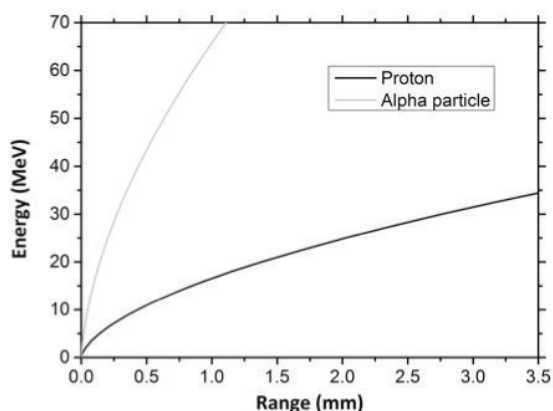


Fig. 4. Calculated ranges of protons and alpha particles in CdTe.

It is worth mentioning that for performing the charged particle discrimination there are two main methods including the rise-time discrimination (Ritcher and Siffert, 1992) and the double pulse shaping methods (Auricchio et al., 2004) available. Since the rise-time measurement methods are generally sensitive to electronic noise and the output of CdTe detectors are rather affected by the electronic noise, the suitable approach for performing charged particle discrimination can be the double pulse shaping method. In this approach, the preamplifier output is shaped with a slow and a fast pulse shaping channels. The slow channel provides the total charge, while the fast channel time constant is set to only partially collect the charge, depending on the rise-time of the input pulse. Consequently, the ratio of the amplitude of the output of the fast channel to that of the slow channel provides information on the type of the particle. From Fig. 5, it is obvious that for thin CdTe detectors, the shaping time constant of the fast channel should be in the range of a few nanoseconds.

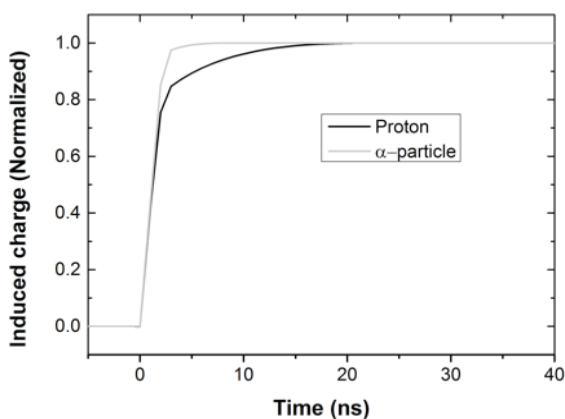


Fig. 5. The shapes of pulses calculated for 5.5 MeV α -particle and protons initiated in a 50 μm thick CdTe detector. The voltage of the detector was 5 volt (1000 V/Cm electric field).

Conclusion

The simplicity, compact size, reliability and relatively low cost of semiconductor detectors like CdTe have made them seem attractive for charged particle discrimination applications. An analysis of the shape of pulses initiated by α -particles and protons in CdTe detector was presented. The results of pulse-shape calculations show that CdTe detectors in conjunction with a fast rise-time charge-sensitive preamplifier can be used for charged particle discrimination of protons and α -particles. For protons and α -particles with energies in excess of about 10 MeV thick detectors can be used for this purpose. At lower energies, detectors with a thickness smaller than the range of protons and larger than the range of α -particles in the detector produce a pulse-shape discrimination property. It has to be mentioned that the usefulness of charged particle response of the detectors can depend on the detector fabrication process, as well as, on the material properties. In fact, heavy charged particles such as α -particles, rapidly lose energy as they pass through a substance, therefore the detector contacts should be very thin, typically being a few hundred nanometers thick to reduce the energy-loss in contact layers.

Conflict of Interest

The author declares that there is no conflict of interest regarding the publication of this article.

Acknowledgements

The author acknowledged the support provided by Deanship of Scientific Research at Majmaah university.

References

- [1]. Sordo, S. D., Abbene, L., Caroli, E., Mancini, A. M., Zappettini, A., and Ubertini, P., 2009. Progress in the Development of CdTe and CdZnTe Semiconductor Radiation Detectors for Astrophysical and Medical Applications. *Sensors* 9 (5), 3491–3526.
- [2]. Takahashi T., and Watanabe S., 2001. Recent progress in CdTe and CdZnTe detectors. *IEEE Transactions on Nuclear Science.*, vol. 48, No. 4, pp. 950-959.
- [3]. Knoll, G. F. 2000. *Radiation Detection and Measurements*, Wiley, New York.
- [4]. Bargholtz Chr., Fumero E., Martensson L., 1999. Model-based pulse shape correction for CdTe detectors. *Nuclear Instrumentation And Methods A* 434, 399.
- [5]. Richter M., Siffert, P., 1992. High resolution gamma-ray spectroscopy with CdTe detector systems. *Nucl. Instrum. and Methods Phys. Res. A* 322, 529-537.
- [6]. Nakhoštin, M., Ishii, K., Kikuchi, Y., Matsuyama, S., Yamazaki, H., Esmaili Torshabiet A., 2009. Time resolution improvement of Schottky CdTe PET detectors using digital signal processing. *Nucl. Instrum. and Methods Phys. Res. A* 606, 681-688.
- [7]. Nishizawa, H., Nishiura, R., Takashima, K., 2004. Position-sensitive detectors based on carrier drift using a CdTe semiconductor. *Nucl. Instrum. and Methods Phys. Res. A* 521, 416-422.
- [8]. Rištinin, R.A., Peterson, R.J., Hamill, J.J., Becchetti, F.D., Entine, G., 1981. An evaluation of CdTe surface barrier diodes as detectors for energetic charged particles. *Nucl. Instrum. and Methods Phys. Res. A* 188, 445-452.
- [9]. Pearson, C. J., Regan, P.H., Divoli, A., 2001. The application of CdZnTe detectors for coincident α - γ spectroscopy. *Nucl. Instrum. and Methods Phys. Res. A* 462, 393-396.
- [10]. Vincent, S.M., Regan, P.H., Owen, K.E., Pearson, C.J., Clough, A.S., 2002. In-beam performance of CdZnTe detectors for proton and alpha-particle measurement. *Nucl. Instrum. and Methods Phys. Res. A* 483, 758-763.
- [11]. Davids, C.N., Back, B.B., Bindra, K., Henderson, D.J., Kutschera, W., Lauritsen, T., Nagame, Y., Sugathan, P., Ramayya, A.V., Walters, W.B., 1992. Startup of the Fragment Mass Analyzer at ATLAS. *Nucl. Instrum. and Methods Phys. Res. B* 70, 358-365.
- [12]. Hetch, K., 1932. *Z Physics*, 77, 235-245.
- [13]. Ziegler, J. F., Biersck, J. P., 1985. *The Stopping Power and Ranges of Ions in Solids*, Pergamon Press, New York.
- [14]. Owen, A., Peacock, A., 2004. Compound semiconductor radiation detectors. *Nuclear Instrum. and Methods Phys. Res. A* 531, 18-37.
- [15]. Auricchio, N., Basili, A., Caroli, E., Donati, A., Franceschini, T., Frontera, F., Hage-Ali, M., Landini, G., Roggio, A., Schiavone, F., Stephen, J.B., Ventura, G., 2004. Compensation of CdZnTe Signals Using a Twin Shaping Filter Technique. *IEEE Trans. Nuclear Science*, Vol. 51, 2485-2491.

Parametric Analysis of Diesel-Brayton Combined Cycle

M.N.Khan

Department of Mechanical and Industrial Engineering, College of Engineering, Majmaah University,
Majmaah 11952, Kingdom of Saudi Arabia
mn.khan@mu.edu.sa

ABSTRACT:

The present study is the comparative parametric energy and exergy analysis of a Proposed Diesel Brayton combined cycle (PCC) and a simple Diesel cycle (DC) by varying the compression ratio (r) and ratio of cut-off to stroke length (k) of Diesel cycle. Proposed Diesel Brayton combined cycle (PCC) consisting of Diesel cycle as topping cycle and Brayton cycle as bottoming cycle which is operated by the exhaust of topping cycle. The result shows that with increase of the compression ratio (r) and ratio of cut-off to stroke length (k), the net output in both PCC and DC increases as well as the exergy loss by the exhaust gasses also increases. The maximum enhancement in net output by PCC is observed as 9.8% at $r = 25$ when $k = 10\%$ as compared to DC.

Keywords: Compression Ratio, Pressure Ratio, Diesel Cycle, Brayton cycle, Exergy loss

1. Introduction

At present, heavy diesel engines are widely used for power generation in the gas turbine power plant for fulfil the peak load and as standbypower supply. Due to the certain limitations of gas turbine as well as steam power plants Diesel power plant is the best option. Diesel engine power plants can be set up quickly, normally in less than twelve months, to generate hundreds of megawatts of energy [1].

But because of structure of internal combustion engine (ICE), it is difficult to fully convert the fuel combustion energy of ICE into the effective power output, and the waste heat from ICE is released into the air via exhaust. Therefore, recovering the waste heat from Diesel engine is an effective way to

improve net output and save fuel. Many researchers have introduced and discussed some kinds of waste heat recovery systems for the stationary ICE. Therefore, combined systems, such as the Organic Rankine cycle (ORC) [2-7] and the Diesel-Kalina cycle [8-11], have been developed for using the waste energy from the engine to produce additional power. The concept of Compound Cycle Engine (CCE) [12] is to utilize the energy of the diesel engine's exhaust for producing extra expansion work, part of which is used in compressing the air prior to the engine's intake manifolds. An extension of the CCE concept which is more relevant to stationary power generation is the combined Diesel-Brayton (CDB) cycle [12-17]. The CDB cycle takes

advantage of the energy content of the diesel-engine's exhaust gas but adds a complete gas-turbine with its compressor and combustion chamber. This arrangement, which enables the diesel engine and gas turbine to be run independently, gives the system great flexibility during operation. While the CDB cycle enables small-scale power generation and industrial cogeneration systems to attain high thermal efficiencies, the fuel flexibilities of diesel engines and gas turbine enables them to be fueled with heavy-diesel fuel, natural gas, or renewable bio-fuels. Mohammadkhani et.al [18] studied the diesel engine based cogeneration system to calculate the exergy destruction within the plant and exergy loss to the environment based on Salvador study [19] and the result shows that fuel utilization efficiency of the overall plant was found to be 90.47% and the exergetic efficiency was 51.08%. The present study describes investigate a comparative parametric analysis of a Proposed Diesel Brayton combined cycle that improves overall energy performance of the combined system with simple Diesel cycle. The cycle under analysis is to optimize the net output of combined cycle and minimize the exergy losses by exhaust gasses from topping cycle by varying the compression ratio (r) of topping (Diesel) cycle and ratio of cut-off to stroke length (k). The performance of diesel cycle depends on compression ratio (r) of topping (Diesel) cycle and duration of heat supply which is technically known as cut-off. The performance of bottoming (Brayton) cycle depends on the temperature of exhaust gasses from the topping cycle. But the temperature of exhaust gasses of diesel cycle is again the function of compression ratio (r) of topping (Diesel) cycle and

ratio of cut-off to stroke length (k). This indicates that the performance of combined cycle is effected by varying the compression ratio (r) of topping (Diesel) cycle and ratio of cut-off to stroke length (k).

Cycle Description

The cycle under analysis is the combination of Diesel cycle as the topping cycle and Brayton cycle as bottoming cycle as shown in fig. 1.

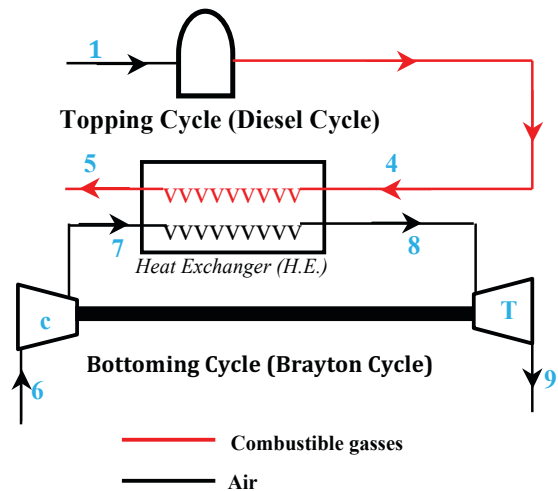


Fig. 1. Schematic diagram of cycle under analysis

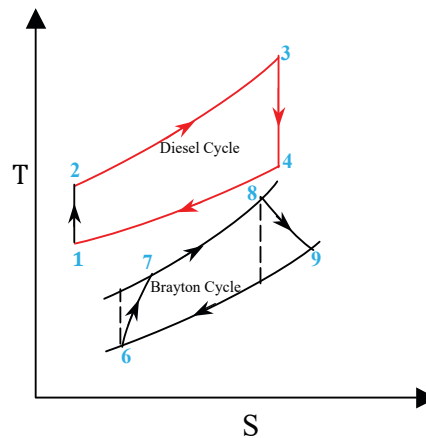


Fig. 2. T-S diagram of cycle under analysis

The bottoming Brayton cycle is operated by the exhaust of Diesel cycle. Air at ambient temperature (T_1) and atmospheric pressure (P_1) enters the Diesel engine and piston moves upward from TDC to BDC and due to this its pressure raises from (P_1) to (P_2) and temperature raises from (T_1) to (T_2).

The combustion process starts when diesel get injected into the high temperature compressed air and due to this combustion the pressure of combustible products raises from (P_2) to (P_3) and temperature raises from (T_2) to (T_3). This high pressure and high temperature of combustible product generate work by moving the piston downward. The combustible product from the diesel engine at the temperature (T_4) leaves to the environment via Heat Exchanger. In bottoming cycle, air at ambient temperature of ($T_6 = T_1$) enters the air compressor where it compressed to the pressure according the pressure ratio (r_p). The high temperature and high pressure air from the air compressor enters the Heat Exchanger where it gains heat from the combustible product of the Diesel engine as per effectiveness of Heat Exchanger. The air at temperature (T_8) and pressure (P_8) enters the turbine via Heat Exchanger where it expands to the pressure (P_9) and leaves to the environment.

Cycle Analysis

Heat supplied to Diesel cycle is given by

$$(Q_s) = m_g \cdot c_{pg} \cdot (T_3 - T_2) \quad (1)$$

Heat rejected by Diesel cycle is given by

$$(Q_R) = m_g \cdot c_{vg} \cdot (T_4 - T_1) \quad (2)$$

Net output from Diesel cycle

$$(W)_{net} = m_g \cdot c_{vg} \cdot \{ \gamma_g (T_3 - T_2) - (T_4 - T_1) \} \quad (3)$$

After putting the value T_2, T_3, T_4 in term of r, ρ and T_1 in equation (3) reduces to

$$(W)_{net} = T_1 \cdot m_g \cdot c_{vg} \cdot \{ \gamma_g \cdot r^{(\gamma_g - 1)} (\rho - 1) - (\rho^{\gamma_g} - 1) \} \quad (4)$$

$$\text{Also } \rho = 1 + k(r - 1) \quad (5)$$

From equation (4) & (5)

$$(W)_{net} = T_1 \cdot m_g \cdot c_{vg} \cdot \left\{ k \cdot \gamma_g \cdot (r - 1) \cdot r^{(\gamma_g - 1)} + 1 - [1 + k(r - 1)]^{\gamma_g} \right\} \quad (6)$$

Temperature of combustible product leaving the Diesel cycle is given by

$$(T_4) = T_1 \cdot \{ 1 + k(r - 1) \}^{\gamma_g} \quad (7)$$

Mass flow rate of fuel in Diesel Engine is given by

$$(m_f) = \frac{T_1 \cdot (m_a)_t \cdot c_{pg} \cdot k \cdot (r - 1) \cdot r^{(\gamma_g - 1)}}{c_v - c_{pg} \cdot T_1 \cdot [1 + k(r - 1)] \cdot r^{(\gamma_g - 1)}} \quad (8)$$

Air Standard Thermal Efficiency of Diesel cycle

$$(\eta_{th})_t = 1 - \frac{[1 + k(r - 1)]^{\gamma_g} - 1}{k \cdot \gamma_g \cdot r^{(\gamma_g - 1)} (r - 1)} \quad (9)$$

$$\text{Let } r_p = (x)^{\frac{1}{(\alpha + \beta)}} \quad (10)$$

Where

$$x = \left(\frac{m_g \cdot c_{pg} \cdot \beta}{(\eta_{th})_t \cdot (m_a)_b \cdot c_{pa} \cdot \alpha \cdot T_6} \right) \cdot T_8$$

$$m_g = (m_a)_t + m_f; \alpha = \frac{\gamma_a - 1}{\gamma_a}; \beta = \frac{\gamma_g - 1}{\gamma_g}$$

Temperature of air leaving the Heat exchanger of bottoming Brayton cycle is given by

$$T_8 = (1 - \varepsilon) \cdot T_7 + \varepsilon \cdot \left(\frac{c_{pg}}{c_{pa}} \right) \cdot T_4 \quad (11)$$

Temperature of air leaving the air compressor of Bottoming cycle is given by

$$T_7 = T_6 \left(1 + \frac{r_p^\alpha - 1}{\eta_c} \right) \quad (12)$$

From equation (10), (11) and (12)

$$T_3 = \left[(1-\varepsilon) \left(1 - \frac{1}{\eta_c} \right) T_6 + \varepsilon \left(\frac{c_p}{c_v} \right) T_6 \right] + \frac{(1-\varepsilon) T_6}{\eta_c} \left[\frac{m_i c_p \beta}{\eta_c (m_i c_p \alpha T_6)} \right]^{\frac{\alpha}{(\alpha-\beta)}} \cdot \frac{1}{(\alpha-\beta)} \quad (13)$$

Temperature of air leaving the turbine of Brayton cycle is given by

$$(T_9) = T_8 (1 - \eta_t (1 - r_p^{-\alpha})) \quad (14)$$

Net output of Bottoming cycle is given by

$$(W_{net})_b = T_6 (m_a)_b c_{pa} \left[T_r \eta_t (1 - r_p^{-\alpha}) - \frac{r_p^\alpha - 1}{\eta_c} \right] \quad (15)$$

Where $T_r = \frac{T_8}{T_6}$

Net output of combined cycle is given by

$$(W_{net})_{comb} = (W_{net})_t + (W_{net})_b \quad (16)$$

Combined Thermal efficiency is given by

$$\eta_{comb} = \frac{(W_{net})_{comb}}{m_f \cdot CV} \quad (17)$$

Exergy loss by the combustible product from the Diesel engine via Heat exchanger is given by

$$(E_{Exh})_{comb} = \int_{T_0}^{T_3} \left(1 - \frac{T_0}{T} \right) dQ \quad (18)$$

Specific Fuel Consumption

$$(SFC)_{comb} = 3600 \cdot \frac{(m_f)}{(W_{net})_{comb}} \quad (19)$$

2. Results and Discussion

The present study is the parametric investigation of variable like compression ratio and the ratio of cut-off to stroke length affecting the performance of Diesel-Brayton combined cycle using first and

second laws of thermodynamics. In topping Diesel cycle it is assumed that the all processes are reversible and no heat leakage is taking place from the engine cylinder to the environment during any process. Whereas in bottoming cycle it is assumed that the pressure drop in the Heat Exchanger is negligible.

Figure 3 shows the variation of net output (W_{net}) of proposed Diesel Brayton combine cycle (PCC) and Simple Diesel Cycle (DC) with respect to compression ratio (r) of Diesel cycle for the range of ratio of cut-off to stroke length (k) from 5% to 10%. It is noted that the net output of the both PCC and DC increases with increase of compression ratio (r) and ratio of cut-off to stroke length (k). It is also noted that at particular value of k the difference of net output of PCC and DC increases with increase of compression ratio (r) and at a particular value of compression ratio (r) the difference of net output of PCC and DC increases with increase of k and the maximum difference occurs at $r = 25$ when $k = 10\%$. The maximum increase in net output of PCC as compared to DC is noted as 9.8% at $r = 25$ when $k = 10\%$.

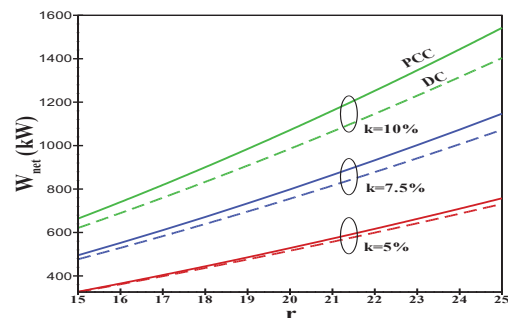


Fig. 3. Variation of Net output (W_{net}) Vs Compression ratio (r) for $k = 5\%$ to 10%

Figure 4 shows the variation of thermal efficiency (η_{th}) of proposed Diesel Brayton combine cycle (PCC) and Simple Diesel Cycle (DC) with respect to compression ratio (r) of Diesel cycle for the range of ratio of cut-off to stroke length (k) from 5% to 10%. It is observed that the thermal efficiency of the both PCC and DC increases with increase of compression ratio (r) and decreases with increase of ratio of cut-off to stroke length (k). Although the thermal efficiency of PCC is much higher than DC and the maximum difference in thermal efficiency of PCC and DC is noted at $r = 25$ when $k = 10\%$. The minimum rise in thermal efficiency of PCC as compared to DC is 0.55% at $r = 15$ when $k = 5\%$ and the maximum rise in thermal efficiency of PCC as compared to DC is 9.9% at $r = 25$ when $k = 10\%$.

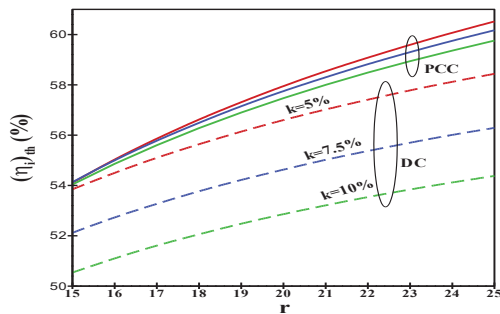


Fig. 4. Variation of Thermal Efficiency (η_{th}) Vs Compression ratio (r) for $k = 5\%$ to 10%

According to equation (19), specific fuel consumption is directly proportional to rate of fuel consumed and inversely proportional to net output of the cycle. Figure 5 shows the variation of specific fuel consumption (SFC) of proposed Diesel Brayton combine cycle (PCC) and Simple Diesel Cycle (DC) with respect to compression ratio (r) of

Diesel cycle for the range of ratio of cut-off to stroke length (k) from 5% to 10%. From fig. 5 it is noted that the specific fuel consumption of both PCC and DC both decreases with increase of compression ratio (r) of Diesel cycle and increases with increase of ratio of cut-off to stroke length (k). The minimum difference in the specific fuel consumption of PCC and DC is noted at $r = 15$ when $k = 5\%$ and the maximum difference in the specific fuel consumption of PCC and DC is noted at $r = 25$ when $k = 10\%$.

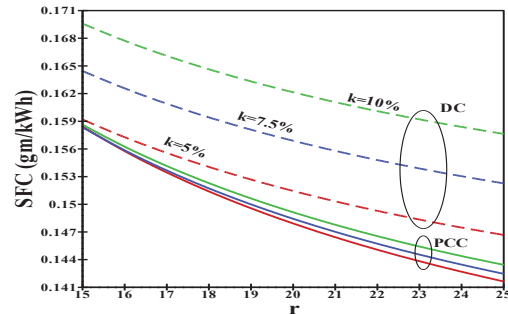


Fig. 5. Variation of Specific Fuel Consumption (SFC) Vs Compression ratio (r) for $k = 5\%$ to 10%

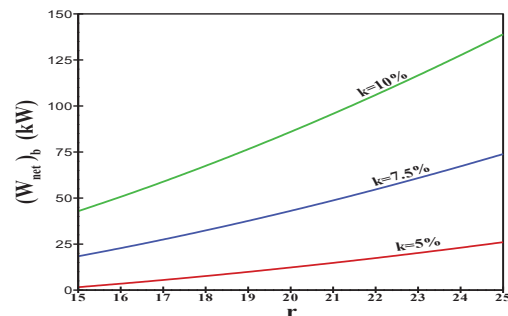


Fig. 6. Variation of Net output (W_{net}) Vs Compression ratio (r) for $k = 5\%$ to 10%

Figure 1 shows that the bottoming (Brayton) cycle is operated by the heat received from the exhaust gasses of topping Diesel cycle. Figure 6 shows the variation of net output (W_{net}) of bottoming Brayton cycle with

respect to compression ratio (r) of Diesel cycle for the range of ratio of cut-off to stroke length (k) from 5% to 10%.

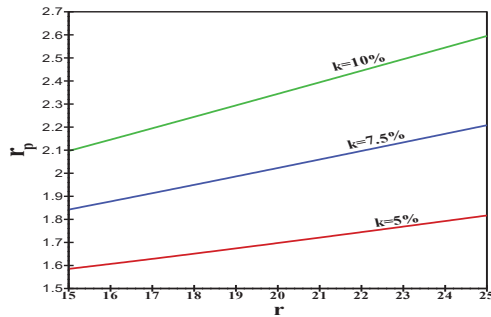


Fig. 7. Variation of Pressure ratio (r_p) Vs Compression ratio (r) for $k = 5\%$ to 10%

The net output of bottoming Brayton cycle increases with increase of compression ratio (r) of Diesel cycle as well as ratio of cut-off to stroke length (k). It is noted that for first 2.5% increase in k , the net output of bottoming cycle increased by 16.78 kW at $r = 15$ and 47.85 kW at $r = 25$ but for second 2.5% increase in k , the net output of bottoming cycle increased by 24.51 kW at $r = 15$ and 65.02 kW at $r = 25$. From equation (7), (10) & (13) it is clear that the pressure ratio of bottoming Brayton cycle is the function of compression ratio (r) of Diesel cycle as well as ratio of cut-off to stroke length (k). Fig. 7 shows the variation of pressure ratio (r_p) of bottoming Brayton cycle with respect to compression ratio (r) of Diesel cycle for the range of ratio of cut-off to stroke length (k) from 5% to 10%. It seems that the pressure ratio increases linearly with increase of compression ratio (r) of Diesel cycle.

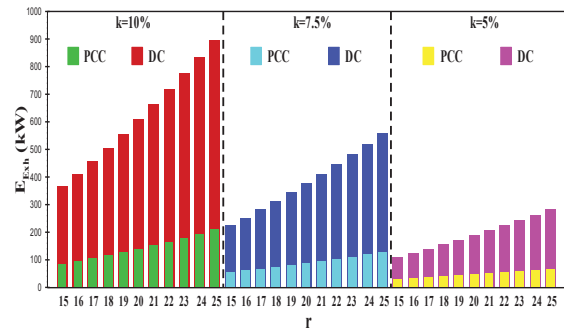


Fig. 8. Variation of Exergy loss by exhaust gases (E_{Ext}) Vs Compression ratio (r) for $k = 5\%$ to 10%

The concept of combined cycle comes in picture to utilize the energy loss by the exhaust gasses of gas turbine cycle so it is very important to study the comparative analysis of exergy loss by exhaust gasses of PCC with DC. Fig.8 shows variation of Exergy loss by combustible product of Diesel engine (E_{Ext}) Vs Compression ratio (r) for $k = 5\%$ to 10% . It is noted that the exergy loss by exhaust gasses increases with increase of Compression ratio (r) of Diesel cycle as well as ratio of cut-off to stroke length (k) but the exergy loss by combustible product of Diesel engine of PCC is much less than the DC. The maximum difference in the exergy loss by the combustible product of Diesel engine between PCC and DC is noted at $r = 25$ when $k = 10\%$ and the minimum difference is noted at $r = 15$ when $k = 5\%$.

Conclusion

Parametric investigation for energy and exergy analysis has been carried out for PCC and DC using 1st and 2nd law of thermodynamic. Heat Exchanger is used to exchange the heat from combustible product of Diesel engine to operate bottoming Brayton cycle

to optimize the net output of combined cycle and minimize the exergy loss by the combustible product of Diesel engine of topping cycle. Based on the analysis as discussed in section 4 the following conclusions have been drawn from this study:

- Compression ratio (r) of Diesel cycle and as well as ratio of cut-off to stroke length (k) play a significant role to increase the net output of both PCC and DC. By PCC the net output increases from 0.5% to 9.8% as compared to DC.
- Thermal efficiency of both PCC and DC increases with increase of Compression ratio (r) and decreases with increase of ratio of cut-off to stroke length (k).
- The difference in net output as well as thermal efficiency between the PCC and DC increases with increase of Compression ratio and ratio of cut-off to stroke length (k).
- The specific fuel consumption of PCC is much less than the specific fuel consumption of DC and decreases with increase of Compression ratio and decrease of ratio of cut-off to stroke length (k).
- The net output of bottoming Brayton cycle increases with increase of Compression ratio and ratio of cut-off to stroke length (k).
- The exergy loss by the exhaust gasses by PCC is much less than DC and the exergy loss by the exhaust gasses of both PCC and DC decreases with decrease of Compression ratio and ratio of cut-off to stroke length (k). The exergy loss by the exhaust gasses from the diesel cycle by PCC decreases from 71% to 77% as compared to DC.

Finally, the PCC is found to be very useful for optimizing the energy conversion performance and minimizing the exergy losses by exhaust gasses.

Nomenclature

W	Work output (kW)
ε	Heat exchanger effectiveness
m	Mass flow rate (kg/s)
Q	Heat supply rate (kW)
η	Thermal efficiency
k	Ratio of cut-off to stroke length
r	Compression Ratio
ρ	Cut-off Ratio
r_p	Pressure ratio
c_p	Specific heat at constant pressure (kJ/kg. K)
c_v	Specific heat at constant volume (kJ/kg. K)
γ	Specific heat ratio
CV	Calorific value of fuel (kJ/kg)
H. E	Heat exchanger
SFC	Specific fuel consumption (gm/kWh)
E	Exergy (kW)
T	Temperature (K)

Subscripts

c	Compressor
cc	Combustion Chamber
T	Turbine
t	Topping Cycle
b	Bottoming cycle
Comb.	Combined cycle
Net	Net
a	Air
g	Gas
Exh.	Exhaust
s	Supply
R	Rejected

References

- [1]. M. Kanoglu, I. Dincer, Performance assessment of cogeneration plants, Energy Conversion and Management 50 (2009) 76–81.
- [2]. V. Doz, R. Novella, A. Garcia, I. Sanchez, HD Diesel engine equipped with a bottoming Rankine cycle as a waste recovery system. Part 1: Study and analysis of the waste heat

- energy, Applied Thermal Engineering 36 (2012) 269-278.
- [3]. Steven Lecompte, Oyeniyi A. Oyewunmi, Christos N. Markides, Marija Lazova, Alihan Kaya, Martijn van den Broek, Michel De Paepe, "Case Study of an Organic Rankine Cycle (ORC) for Waste Heat Recovery from an Electric Arc Furnace (EAF)", Energies 2017, vol.10, 3-16.
- [4]. Md. A. A. Mamun, Subrato Biswas, "Waste Heat Recovery System by Using an Organic Rankine Cycle (ORC)", International Journal of Scientific & Engineering Research, Volume 3, Issue 10, October-2012, 1-4.
- [5]. Alison Auld Arganthaël Berson Simon Hogg, "Organic Rankine cycles in waste heat recovery: a comparative study" International Journal of Low-Carbon Technologies, Volume 8, Issue suppl_1, 1 July 2013, 9-18.
- [6]. Suresh Baral, Kyung Chun Kim, "Simulation, Validation and Economic Analysis of Solar Powered Organic Rankine Cycle for Electricity Generation", Journal of Clean Energy Technologies, Vol. 3, No. 1, January 2015
- [7]. Nattaporn Chaiyat, "Assessment Alternative Energy for Organic Rankine Cycle Power Plant in Thailand", International Journal of Engineering and Technology (IJET), Vol 7 No 1 Feb-Mar 2015.
- [8]. M. Jonsson, J. Yan, Exergy and Pinch Analysis of Diesel Engine Bottoming Cycles with Ammonia-Water Mixtures as Working Fluid, Int. J. Applied Thermodynamics, Vol.3 (No.2), (2000), 57-71.
- [9]. Paola Bombarda, Costante M. Invernizzi, Claudio Pietra, "Heat recovery from Diesel engines: A thermodynamic comparison between Kalina and ORC cycles", Applied Thermal Engineering Volume 30, Issues 2–3, February 2010, Pages 212-219.
- [10]. Mohamed M. El-Awad, "Energy and Exergy Analysis of a combined Diesel-Engine Gas-Turbine System for Distributed Power Generation", Int. J. of Thermal & Environmental Engineering Volume 5, No. 1 (2013) 31-39.
- [11]. Jianyong Wang, Jiangfeng Wang, Pan Zhao, Yiping Dai, Yan Peng, "Thermodynamic Analysis and Comparison Study of an Organic Rankine Cycle (ORC) and a Kalina Cycle for Waste Heat Recovery of Compressor Intercooling" ASME Turbo Expo 2014: Turbine Technical Conference and Exposition June 16–20, 2014, pp.7-10.
- [12]. G.A. Bobula, W.T. Wintucky W and J.G. Castor, Compound Cycle Engine Program, NASA Technical Memorandum 88879, Prepared for the Rotary Wing Propulsion System Specialist Meeting sponsored by the American Helicopter Society Williamsburg, Virginia, November 12- 14, 1986.
- [13]. S. Mukul, R. Agarwal, Energy and Exergy Analysis of Brayton-Diesel Cycle, Proceedings of the World Congress on Engineering Vol II, July 1 - 3, 2009, London, U.K.
- [14]. S.S. Krishna, C.J.T. Renald, Numerical analysis of a turbo compounded Diesel – Brayton combined cycle, Continuum Mechanics, Fluids, Heat, (2010), 258- 261.
- [15]. Balli, O., Aras, H., Hepbasli, A., "Thermodynamic and thermoeconomic analyses of a trigeneration (TRIGEN) system with a gas–diesel engine: Part I – Methodology", Energy Conversion and Management, vol. 51, pp. 2252–2259, 2010
- [16]. Abusoglu, A., Kanoglu, M., "Exergetic and thermoeconomic analyses of diesel engine powered cogeneration: Part 2 – Application", Applied Thermal Engineering, vol. 29, pp. 242–249, 2009.
- [17]. Abusoglu, A., Kanoglu, M., "Exergetic and thermoeconomic analyses of diesel engine powered cogeneration: Part 1 – Formulations", Applied Thermal Engineering, vol. 29, pp. 234–241, 2009.
- [18]. F. Mohammadkhani, Sh. Khalilarya, I. Mirzaee, "Energetic and Exergetic Analysis of Internal Combustion Engine Cogeneration System" The Journal of Energy: Engineering & Management Vol. 2, No. 4, Winter 1391, P. 24-31.
- [19]. Salvador, M.A., Joel, M.F., Gordon, M.R., "Analysis of Homogeneous Charge Compression Ignition (HCCI) engines for cogeneration applications", Journal of Energy Resources Technology, vol. 128, 2006

Journal of Engineering and Applied Sciences (JEAS)

- **Improved Performance of Doppler Tolerant Radars Using Digital Code**

Saud S. Alotaibi

- **Simulation Study on Charged Particle Discrimination Properties of CdTe Detectors**

T. Alharbi

- **Parametric Analysis of Diesel-Brayton Combined Cycle**

M.N.Khan